AAS 15-594

ANALYTICAL LOW-THRUST TRANSFER DESIGN BASED ON VELOCITY HODOGRAPH

D.J. Gondelach [*], and R. Noomen [†]

Shape-based models can be used to approximate low-thrust transfer orbits between celestial bodies. Here, a new model is proposed, which is based on simple analytical base functions that together represent the velocity of the spacecraft. After integration, these base functions also yield analytical expressions for distances traveled. As a result, both the velocity and the trajectory of a transfer can be modeled analytically with a series of such base functions, which can be chosen and scaled at will. Constraints (*i.e.* conditions on initial and final position and velocity) can be satisfied directly, and a constraint on the final polar angle can be met with a straightforward, fast numerical integration. The technique allows for direct solutions with no degrees of freedom, but also facilitates a more extensive analytical modeling where certain aspects of the resulting transfer trajectory (*e.g.* required ΔV, maximum acceleration) can be optimized. The main characteristics of the technique are illustrated in a number of cases: transfers to Mars and Mercury.

INTRODUCTION

By virtue of their efficiency, low-thrust rocket engines are very attractive for interplanetary missions: large amounts of ΔV are typically required, which can be achieved by virtue of the long flight times (even though we deal with very small accelerations). However, the degrees of freedom of such transfers pose a big challenge for the design of the optimal trajectory.

Although they have limitations in terms of accuracy, analytical methods play an important role in interplanetary trajectory design: they are fast, and help to reduce the search space for full numerical optimizations significantly. In particular, shape-based techniques have become very popular during the past decades. Examples are exponential sinusoids,[1,2] inverse polynomials,[3,4,5] pseudo-equinoctial shaping,[6,7,8] spherical shaping,[8] finite Fourier Series[9,10] and the pseudo-spectral method.[11] They all describe the shape of the transfer by means of a mathematical expression with a limited number of parameters, and the required thrust to fly such a transfer is obtained by confrontation with the equations of motion. A summary of the performance of such methods is given in Table 1. Although elegant, almost all of them have limitations on boundary conditions, dimensionality and/or maximum thrust. The single exception appears to be the pseudo-spectral technique.

This paper presents a low-thrust shaping method which is based on velocity hodographs. Here, boundary conditions on velocity at departure and arrival at the destination can be met directly. A

[*] PhD Student, Faculty of Engineering and the Environment, University of Southampton, Highfield, Southampton, SO17 1BJ Hampshire, United Kingdom, davidgondelach@gmail.com

[†] Assistant Professor, Faculty of Aerospace Engineering, Delft University of Technology, Kluyverweg 1, 2629 HS, Delft, The Netherlands

Table 1. Comparison of shape-based methods for low-thrust trajectory design; † solved without iterations or constraint optimization, ‡ using constraint optimization, * only valid for small inclination changes.

Method	Boundary conditions		Time of flight	3D	Thrust
	Position	Velocity	solved directly†		acceleration limit
Exposin	Yes	No	No	No	No
Inverse polynomial	Yes	Yes	No	Yes*	No
Spherical	Yes	Yes	No	Yes	No
Pseudo-equinoctial	Yes	Yes	No	Yes	Yes‡
Fourier series	Yes	Yes	Yes	No	Yes
Pseudo-spectral	Yes	Yes	Yes	Yes	Yes‡

main feature of the technique is that the velocity modeling can easily and analytically be transfered to the position domain, *i.e.* the trajectory; boundary conditions on position are also met directly.

First, this paper discusses the theory of this novel hodographic-shaping method in detail. The implementation and test cases will be treated next. The technique is applied to two test cases: a mission to Mars (a more outer planet) and a mission to Mercury (a more inner planet); these cases have different implications for the modeling of the transfer. The paper ends with conclusions.

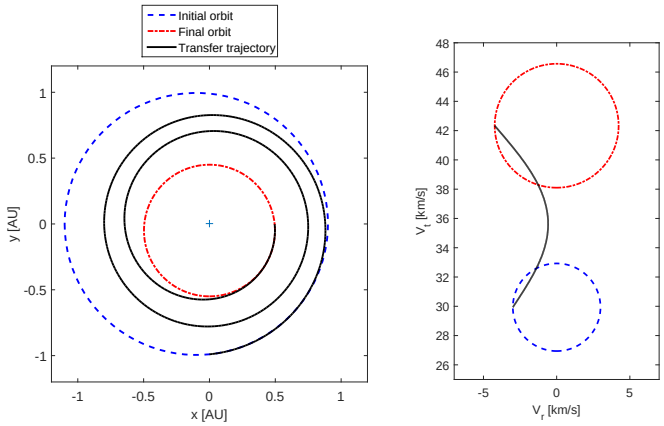

Figure 1. Transfer trajectory with the initial and final orbit (left) and corresponding velocity hodographs (right).

THEORY

Typically, shape-based methods start from the concept of shaping position, *i.e.* trajectories, and then address constraints on *e.g.* velocities. For our technique, we do the reverse: we start by modeling the velocity behavior of a low-thrust trajectory, and then develop this into the position domain. Fig. 1 gives an illustration of velocity hodographs: the right-hand plot shows the hodograph of an arbitrary high initial (blue) and a low final (red) orbit around the Sun (both are non-circular). The black line indicates the velocity behavior of a possible transfer between these two orbits. Clearly, this path matches the velocities of the two orbits at two (arbitrary) instances, or, formulated differently, it satisfies the rendezvous conditions on initial and final velocity. The fundamental idea of the

velocity hodograph for shaping low-thrust transfers is that their velocity behavior can be described by a simple analytical model. By integrating such a velocity profile, the variation in position can be obtained and the initial and final boundary conditions on position can be satisfied as well.

It is logical to shape velocity as a function of time, since physical velocities are time rates of change. However, it is also possible to shape the rates of change in position as a function of the polar angle θ. Both a time-driven and polar-angle-driven method have been developed.[12,13] However, in the current paper we will focus on the time-driven approach (although some results obtained with the polar-angle-driven implementation will also be shown).

In our model, the 3-dimensional velocity is represented with cylindrical coordinates r, θ and z. Angular coordinates would lead to complicated expressions for velocity (and position), leading to unnecessarily tedious formulations to meet boundary conditions. Cartesian coordinates are clearly also not a good choice, as they vary too much over time.

In cylindrical coordinates the equations of motion are as follows:

$$\ddot{r} - r\dot{\theta}^2 + \frac{\mu}{s^3} r = f_r \tag{1}$$

$$r\ddot{\theta} + 2\dot{r}\dot{\theta} = f_\theta \tag{2}$$

$$\ddot{z} + \frac{\mu}{s^3} z = f_z \tag{3}$$

where $s = \sqrt{r^2 + z^2}$ is the distance from the central body, and the terms on the right-hand side represent the accelerations generated by the rocket engine. The dynamics of the transfer are driven by the gravitational acceleration by the Sun and the thrust acceleration only (all other accelerations are several orders of magnitude smaller). Obviously, we only consider interplanetary cases here.

Basics

In the time-driven method, the radial, transverse and axial velocities (V_r, V_θ and V_z, respectively) are shaped as a function of time t: $V_r = V_r(t)$, $V_\theta = V_\theta(t)$ and $V_z = V_z(t)$. The radial and axial distances are obtained by analytical integration of the radial and axial velocities:

$$r(t) = r_0 + \int_0^t V_r dt, \quad z(t) = z_0 + \int_0^t V_z dt \tag{4}$$

whereas the polar angle can be derived by integrating the angular velocity:

$$\theta(t) = \theta_0 + \int_0^t \dot{\theta} dt = \theta_0 + \int_0^t \frac{V_\theta}{r} dt \tag{5}$$

However, numerical integration is required to compute the (final) polar angle. More on this is discussed in a subsequent subsection.

By substituting V_r, V_θ and V_z and their derivatives and integrals into the equations of motion Eqs. (1) to (3), the individual components of the required thrust acceleration can be computed. Finally, the required total ΔV is obtained by numerically integrating the thrust acceleration f:

$$\Delta V = \int_0^{t_f} f dt = \int_0^{t_f} \sqrt{f_r^2 + f_\theta^2 + f_z^2} dt \tag{6}$$

Velocity functions

Shape-based methods are typically used for a fast first-order assessment of interesting transfer options, which can be refined in a subsequent numerical optimization. Clearly, efficiency is crucial here. Therefore the formulations for velocity as well as their derivatives and integrals need to be simple analytical expressions as much as possible. We have chosen to model velocity as a sum of simple terms, called base functions: polynomial, trigonometric and exponential terms (to be discussed further in a following subsection). Clearly, they all can be integrated analytically. Essentially, an arbitrary velocity function consists of a sum of such base functions v_i, scaled with coefficients c_i:

$$V(t) = \sum_{i=1}^{n} c_i v_i(t) \tag{7}$$

In principle, the number of base functions n can be chosen at will for any velocity component (radial, transverse, axial) and can be different for each of these three directions. However, the minimum number of base functions required per velocity function is equal to the number of boundary conditions that have to be satisfied by that particular velocity function.

Boundary conditions

Each velocity function $V(t)$ has to satisfy three boundary conditions: two on initial and final velocity, V_0 and V_f, and one on the difference between the initial and final position, $P_f - P_0$. In total nine boundary conditions need to be satisfied:

$$\begin{aligned}
&V_r(0) = V_{r,0}, \quad V_r(t_f) = V_{r,f}, \quad \int_0^{t_f} V_r dt = r_f - r_0, \\
&V_\theta(0) = V_{\theta,0}, \quad V_\theta(t_f) = V_{\theta,f}, \quad \int_0^{t_f} \frac{V_\theta}{r} dt = \theta_f = \psi + 2\pi N, \\
&V_z(0) = V_{z,0}, \quad V_z(t_f) = V_{z,f}, \quad \int_0^{t_f} V_z dt = z_f - z_0
\end{aligned} \tag{8}$$

The subscripts 0 and f indicate initial and final conditions, respectively, $\psi \in [0, 2\pi)$ is the transfer angle, and $N = 0, 1, 2...$ is the number of complete revolutions. Since three conditions per velocity function need to be met, the first three coefficients of each velocity function $V(t)$ are used to satisfy these. The equations which need to be solved can be written in matrix form as follows:

$$\begin{aligned}
&\begin{bmatrix} v_1(0) & v_2(0) & v_3(0) \\ v_1(t_f) & v_2(t_f) & v_3(t_f) \\ \tilde{v}_1(t_f) - \tilde{v}_1(0) & \tilde{v}_2(t_f) - \tilde{v}_2(0) & \tilde{v}_3(t_f) - \tilde{v}_3(0) \end{bmatrix} \begin{bmatrix} c_1 \\ c_2 \\ c_3 \end{bmatrix} \\
&\qquad = \begin{bmatrix} V_0 - \sum_{i=4}^{n} c_i v_i(0) \\ V_f - \sum_{i=4}^{n} c_i v_i(t_f) \\ P_f - P_0 - \sum_{i=4}^{n} c_i [\tilde{v}_i(t_f) - \tilde{v}_i(0)] \end{bmatrix}
\end{aligned} \tag{9}$$

The tilde symbol indicates the integral with respect to time. In principle, after picking values for n and c_i (i=4,...n), one can solve Eq. (9) for the coefficients c_1 to c_3 provided the matrix on the left-hand side of the equation is invertible. Clearly, this must be done for each velocity component separately. For the transverse component the boundary conditions are satisfied differently, which will be discussed in the following subsection.

Final polar angle condition

For the transverse direction, two direct boundary conditions on the transverse velocity itself exist: initial and final velocity. The values of c_1 and c_2 can be found using:

$$\begin{bmatrix} v_1(0) & v_2(0) \\ v_1(t_f) & v_2(t_f) \end{bmatrix} \begin{bmatrix} c_1 \\ c_2 \end{bmatrix} = \begin{bmatrix} V_0 - c_3 v_3(0) - \sum_{i=4}^{n} c_i v_i(0) \\ V_f - c_3 v_3(t_f) - \sum_{i=4}^{n} c_i v_i(t_f) \end{bmatrix} \tag{10}$$

Rearranging terms results in:

$$\begin{bmatrix} c_1 \\ c_2 \end{bmatrix} = c_3 \begin{bmatrix} v_1(0) & v_2(0) \\ v_1(t_f) & v_2(t_f) \end{bmatrix}^{-1} \begin{bmatrix} -v_3(0) \\ -v_3(t_f) \end{bmatrix} + \begin{bmatrix} v_1(0) & v_2(0) \\ v_1(t_f) & v_2(t_f) \end{bmatrix}^{-1} \begin{bmatrix} V_0 - \sum_{i=4}^{n} c_i v_i(0) \\ V_f - \sum_{i=4}^{n} c_i v_i(t_f) \end{bmatrix} \tag{11}$$

or, in short-hand notation:

$$\begin{bmatrix} c_1 \\ c_2 \end{bmatrix} = c_3 \begin{bmatrix} K_1 \\ K_2 \end{bmatrix} + \begin{bmatrix} L_1 \\ L_2 \end{bmatrix} \tag{12}$$

As for the position in transverse direction, this is expressed by the polar angle θ. To obtain this angle, one needs to integrate the angular velocity $\dot{\theta}$ over time. However, this integral, Eq. (5), can in general not be computed analytically and therefore the boundary condition on position needs to be solved in a numerical way. Fortunately, this can be done without iterative calculations.

The following condition for the final polar angle has to be satisfied:

$$\int_0^{t_f} \dot{\theta} dt = \int_0^{t_f} \frac{V_\theta}{r} dt = \int_0^{t_f} \frac{c_1 v_1 + c_2 v_2 + c_3 v_3 + \sum_{i=4}^{n} c_i v_i}{r} dt = \theta_f \tag{13}$$

The solutions for c_1 and c_2 (Eq. (12)) are substituted into Eq. (13) to obtain an equation with c_3 as the only unknown. After some rearranging, the value for c_3 which satisfies the final polar angle condition can readily be obtained:

$$c_3 = \frac{\theta_f - \int_0^{t_f} \frac{L_1 v_1 + L_2 v_2 + \sum_{i=4}^{n} c_i v_i}{r} dt}{\int_0^{t_f} \frac{K_1 v_1 + K_2 v_2 + v_3}{r} dt} \tag{14}$$

The boundary conditions on the transverse velocity function can now be solved using Eqs. (12) and (14). The computational effort required is still little since no iterations are needed.

Base functions

The velocity functions are built up as a sum of simple mathematical terms v_i (Eq. (7)) which can be differentiated and integrated analytically. These simple functions are called base functions, and they can for example be a sine, cosine, power, exponential, or multiplication of a power with a sine or cosine term, as long as they are analytically differentiable and integrable. The options investigated here are summarized in Table 2.

Early investigations revealed that it is useful to normalize the driving parameter t by dividing by the final value t_f (time of flight, TOF). So, the range of t/t_f over the trajectory is $[0, 1]$. The main benefit of this scaling is that the magnitude of the different base functions is similar. As a result,

the coefficients c_i are similar in magnitude, which makes optimization using extra coefficients more robust. An exception for this scaling is made for trigonometric base functions. This makes the polar-angle trigonometric functions one-revolution periodic.

Elapsed time, however, is not related to the geometry. For the time-driven method it was chosen to scale time by a factor $2\pi n/t_f$ for trigonometric functions such that these functions complete n periods as time runs from 0 to t_f.

Table 2. Base functions, their derivatives and integrals.

Base function	$v(t)$	$\frac{dv}{dt}$	$\int v dt$
Constant	1	0	t
Power	t^n	nt^{n-1}	$\frac{1}{n+1}t^{n+1}$
Sine	$\sin(nt)$	$n\cos(nt)$	$-\frac{1}{n}\cos(nt)$
Cosine	$\cos(nt)$	$-n\sin(nt)$	$\frac{1}{n}\sin(nt)$
Power times sine	$t^m \sin(nt)$	see Gondelach[12]	
Power times cosine	$t^m \cos(nt)$	see Gondelach[12]	

In principle, any combination of base functions can be used to form a velocity function, as long as the boundary conditions can be met. Of course, the resulting trajectory depends on the chosen velocity functions. Therefore a proper combination of base functions needs to be made to obtain good trajectories concerning required ΔV and/or thrust acceleration. This will be discussed later.

As mentioned earlier, a minimum of three base functions are required to satisfy the boundary conditions, per velocity function (*i.e.* per dimension). Such a set is called a zero-order solution. Such solutions can be improved by adding additional base functions to the velocity functions (*i.e.* $n > 3$) (cf. Eq. (7)). These extra terms result in extra degrees of freedom (DoF) and all extra coefficients c_i can be estimated to obtain (near-)optimal trajectories ($c_{1,2,3}$ still satisfying Eqs. (9), (12) and (14) of course). A solution which contains extra terms is called a higher-order solution. The extra DoF make the shape of velocity functions more flexible and therefore can be expected to result in better trajectories. This flexibility, however, comes at the cost of computational effort, since optimization is required.

In this paper the extra coefficients are used to minimize the required ΔV. Of course, they can also be used to minimize flight time, or satisfy a thrust acceleration constraint.

IMPLEMENTATION

In the remainder of this report, base functions will be abbreviated in order to express velocity functions shortly. The way of abbreviating is shown in Table 3. For example, one expresses $1+t^2+\cos(2\pi t)$ as CPow2Cos. Also, the coding will express the functions in radial, transverse and axial directions: CPow2-Cos05-P3CosR5 means $1+t^2$ for radial, $\cos(\pi t)$ for transverse and $t^3\cos((N+0.5)*2\pi t)$ for axial velocity, respectively.

Integration

For the computation of the required total ΔV and for satisfying the condition on the final polar angle, numerical integration is required (cf. Eqs. (6) and (14), respectively). Obviously, the effort to do such an integration should be minimal. Not only does this concern the computational effort when doing a straightforward 0-DoF calculation (*i.e.* only one set of calculations), but this is even more

Table 3. Abbreviations used for base functions; † 05 refers to the factor 0.5 and R5 refers to the factor $N + 0.5$, where N is the applied number of revolutions.

Base function	Abbreviation	Base function	Abbreviation
1	C	$\cos(2\pi t)$	Cos
t	Pow	$\cos(N * 2\pi t)$	CosR †
t^2	Pow2	$t \sin(2\pi t)$	PSin
t^5	Pow5	$t^2 \cos(2\pi t)$	P2Cos
$\sin(2\pi t)$	Sin	$t^3 \sin(1.5 * 2\pi t)$	P3Sin15
$\sin(0.5 * 2\pi t)$	Sin05 †	$t^6 \cos((N + 0.5) * 2\pi t)$	P6CosR5 †

important when introducing a number of DoF, in which case hundreds of different options need to be evaluated in an optimization scheme. A number of test cases has been used for this purpose;[12] here we only report about a 2-dimensional transfer from Earth to Mars, where an arbitrary value for the TOF of 3 years is assumed, and the radial and transverse velocities are modeled with CCosPowSin and CPowSin, respectively. Results have been obtained for the following number of integration steps: 10, 15, 20, 25, 50, 100 and 1000. Taking the latter as the obvious reference, the errors in the results for any other number of steps can be assessed. It turned out that 25 integration steps is the best choice: the resulting total ΔV perfectly matches the result for 1000 steps, whereas the final polar angle shows an error of a mere 0.3×10^{-6} rad, equivalent to a very acceptable position error when arriving at Mars of about 68 m. Similar results were obtained for test cases on transfers to Mercury and comet Tempel 1.[12]

Optimization

As mentioned before, in case higher-order solutions are investigated, the trajectories are optimized for minimum ΔV. The general procedure adopted here is to investigate the problem with a grid-search technique, where the steering parameters, launch date and TOF, are sampled in a regular way (*e.g.* with steps of 20 days each) and the transfer for any individual combination of parameters is optimized with the Nelder-Mead (NM) algorithm as implemented by O'Neill.[14] NM was found to be faster than other optimization techniques (*e.g.* Differential Evolution), especially for low-ΔV trajectories. In addition, NM appeared to be more robust in case the number of objective function evaluations is limited and the number of DoF is not more than six.

As for NM, a maximum of 5000 function evaluations was allowed (much less was actually needed) and as initial guesses for the free parameters the optimal values of a neighboring solution (in terms of departure date and TOF) were used. To illustrate the latter, we use the transfer from Earth to Mars. Of course, it is expected that some combinations of launch date and TOF will reveal attractive if not optimal transfers, and that (many) other pairs will result in inefficient transfers. To get an idea of the quality of the results, we first investigated the sensitivity of the resulting transfer trajectory to the governing input parameters. Fig. 2 shows the solutions for the scaling factors of the base functions for a mission to Mars with arbitrary (but fixed) departure date, $N = 2$ (*i.e.* two full revolutions) and varying TOF. For each combination of departure date and TOF, the results are optimized for minimum ΔV.

Clearly, this holds for a higher-order solution; the velocity model is as illustrated in the caption (with more base functions per coordinate than the minimum required three). A number of aspects can be recognized in this plot. First, the solutions for parameters c_i do vary with TOF, but in a very

smooth way. Since the optimization of the problem (here and in the remainder of this paper) is done with a combination of a grid search and the NM technique, it is attractive to use the solution of the previous point evaluated in this grid as initial conditions for a new neighboring pair. More specifically, this is done for subsequent samples of TOF rather than samples in departure date, since the latter was found to cause more variation in the results. This influences the efficiency of the NM optimization in a (very) positive way. Second, the smoothness in the patterns is apparently broken at TOF values of about 970 and 1670 days, respectively. These discontinuities are the result of a significant change in the geometry of the problem: at these TOFs, the value of the transfer angle ψ reaches its upper bound of 2π and changes to 0 since it must be in the range $[0, 2\pi)$. As a consequence, the final polar angle condition changes discontinuously. Obviously, the occurrence of this phenomenon repeats approximately after the synodic period of the Earth-Mars constellation.

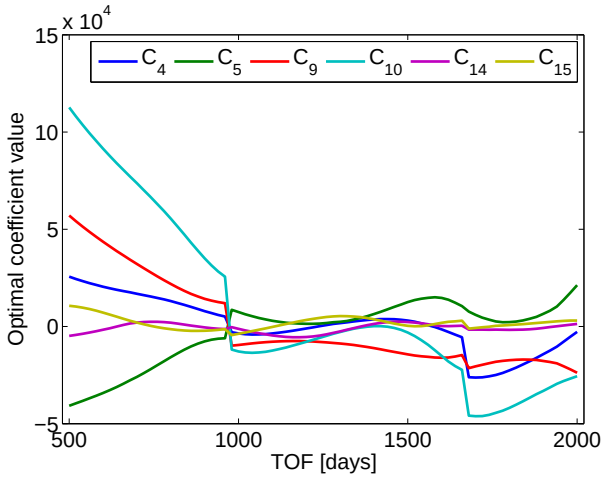

Figure 2. Solutions for all extra coefficients c_i for a mission to Mars, for different values of TOF. $N = 2$, departure date is 8705 MJD2000 and V_r = CPowPow2PSin05PCos05, V_θ = CPowPow2PSin05PCos05, V_z = CosR5P3CosR5P3SinR5P4CosR5P4SinR5.

To further increase the speed of the optimization, the base function values at the integration points are cached. For a fixed TOF, departure date and number of revolutions the base functions as well as their derivatives and integrals purely depend on time. Therefore, if the integration points are fixed, the base function values at these points are fixed and they need to be computed only once and can be stored. With these cached values, solving the boundary conditions and computing the required ΔV for different values of the free parameters can be done very quickly. As a result, the optimization takes very little time: a factor of up to 50 w.r.t. the non-cached approach is gained. Clearly, this holds for the situation with extra degrees of freedom, and where optimization is performed.

Verification

The hodographic-shaping method has been verified by numerically propagating the initial spacecraft state vector using the thrust-acceleration profile found by the shaping method. In particular, this has been done for a transfer from Earth to Mercury, with a time of flight of 2 years, and both radial and transverse velocity taken to be CPowCosSinSin2Sin3Cos2Cos3Pow2Pow3PSinPCos. The latter choice is completely arbitrary, but is done to make velocity and trajectory more complicated. For the numerical propagation, the same initial position and velocity as for the hodographic shaping

method have been used, and therefore these are identical by definition. For the computation of the ΔV and the final polar angle in the shaping method, 2.0 $\times 10^6$ integration steps were used. This guarantees that the results of the shaping method are not erroneous due to integration errors. For the same reason, a very large number of steps was chosen for the numerical propagation.

The shaping method and the numerical propagation based on the thrust profile give identical results: the differences in final radius, angular position, radial and angular velocity and total ΔV are all about 11 orders of magnitude smaller than the results themselves (*e.g.* the difference in final radial distance is 1.7 $\times 10^{-4}$ km, the difference in ΔV is 4.9 $\times 10^{-9}$ km/s). Negligible as they are, these residual errors are probably related to integration errors in either of the two approaches (hodograph and numerical). The polar-angle-driven method has been tested and evaluated in a similar way and with similar quality of results.[12,13]

Fig 3 shows the trajectory and the velocity hodograph of the transfer to Mercury, corresponding to the Earth-Mercury test case described above. The trajectory is given in an inertial heliocentric reference frame, and seems far from realistic. However, the trajectory does fulfill the initial and final boundary conditions on position and velocity and is therefore perfectly valid (in spite of the huge ΔV of 215.9 km/s). We apparently defined an unattractive transfer (the values of the extra coefficients were obtained by a random generator, and not optimized). Independent of the quality of the result, the hodographic shaping method gives correct results.

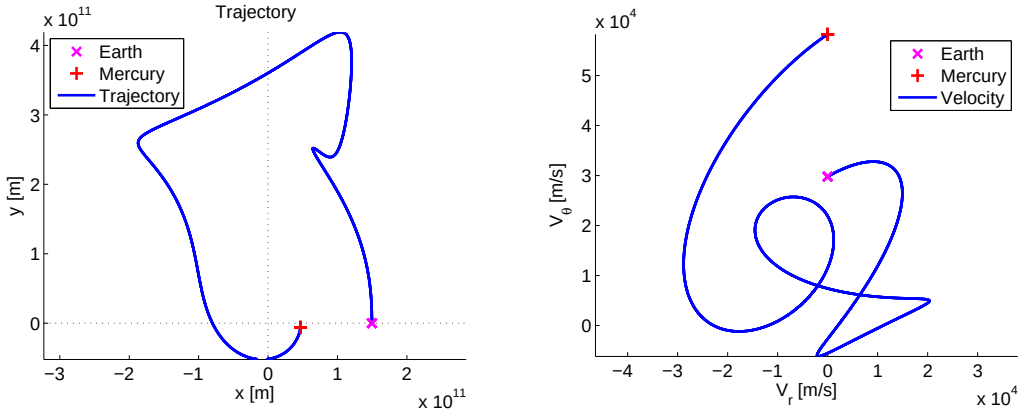

Figure 3. Trajectory (left) and velocity hodograph (right) corresponding to the test trajectory from Earth to the pericenter of Mercury.

To further illustrate results and potential pitfalls, Fig. 4 shows the thrust-acceleration profile of a good (*i.e.* low ΔV) and a bad (*i.e.* high ΔV) trajectory to Mercury. The thrust acceleration in Fig. 4(a) does not change very gradually, but is smooth and restricted in magnitude. The profile in Fig. 4(b) however contains two asymptotic spikes and is clearly not smooth. The spikes are singularities caused by the fact that the spacecraft flies "through" the Sun, first to a negative radial distance and subsequently back to a positive radial distance. Obviously, such a behavior for distance is physically impossible, and this candidate trajectory must be considered as unfeasible. A numerical integrator with a relatively large step size can easily misjudge the height of these spikes (cf. Eq. (6)), and as a consequence the required ΔV is estimated incorrectly. Nevertheless, because the thrust acceleration is extremely high around the spikes, the estimated ΔV will be very large. Since good transfer trajectories are not expected to exhibit thrust profiles with singularities or high spikes,

the integration errors for these trajectories are small. Indeed, it was found that the error in estimated ΔV is large for bad transfers and small for good ones. Infeasible trajectories may be encountered during optimization, but will be overruled by physically correct ones with lower ΔV.

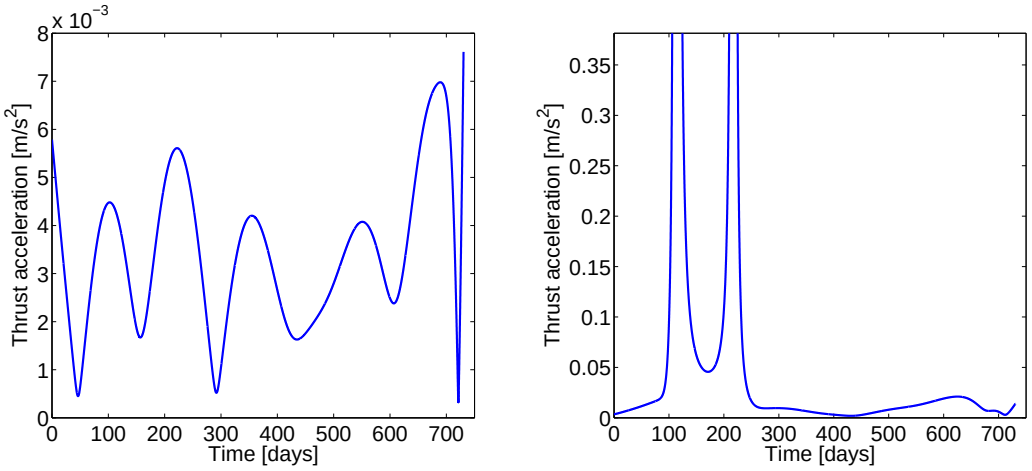

Figure 4. Thrust acceleration for a feasible (left) and an unfeasible (right) trajectory to Mercury; the latter one requires an infinite thrust acceleration at two instances.

CASES

Introduction

In order to better understand the possibilities and potential drawbacks of the hodographic-shaping method, two cases have been investigated in detail: a rendezvous mission from Earth to Mars, and a similar one to Mercury. The Mars case can be regarded as a relatively easy problem, with a small eccentricity and inclination of the destination orbit, and an expected smooth behavior of parameters of the transfer orbit. The Mercury case is different: larger values for e and i, and a faster rotation around the Sun (consequently, a problem with higher velocities, different periodicities, and such). These two cases are expected to reveal different aspects of the velocity-hodograph technique.

In addition, these two cases have been selected because other investigators have already analyzed them independently. The Mars mission has been used to test the spherical-shaping and pseudo-equinoctial-shaping methods.[8] The mission to Mercury has been used to evaluate the pros and cons of the pseudo-equinoctial-shaping method.[6] In addition, external results were obtained using DITAN, a state-of-the-art optimization tool for low-thrust interplanetary trajectory design.[7]

The orbital elements of the three planets have been taken from JPL Solar System Dynamics[†].

The used ranges for launch windows and time of flight are given in Table 4, and are identical to the ones applied by Novak and Vasile[8] and De Pascale and Vasile.[6] Initial calculations were done for a grid spanned by time of departure and TOF with step sizes of 10 and 20 days for zero-order and higher-order solutions, respectively.

In both cases, the time-driven as well as the polar-angle-driven method has been investigated.[12,13]

[*]Data available online at `http://ssd.jpl.nasa.gov/` [retrieved 8 June 2012].

Table 4. Departure date and TOF ranges of flight windows for different cases and orbital and synodic periods of target bodies (with respect to Earth).

	Departure date [MJD2000]	TOF [days]	Orbital period [days]	Synodic period [days]
Mars	7304 - 10225	500 - 2000	687	780
Mercury	3285 - 5475	100 - 1400	88	116

However, in this paper we will mainly focus on the results obtained with the first technique. In particular, the results that can be obtained with different velocity functions (both in case of zero-order and higher DoF) will be presented and discussed. The best results are mainly compared on the aspects required ΔV, maximum thrust acceleration, departure date and TOF. For obvious reasons, Pareto fronts are used to illustrate the most attractive solutions obtained for different methods and different velocity functions.

Mars

The first case studied is the transfer from Earth to Mars. Such a transfer, easy and smooth as it may seem, still reflects a number of aspects of the velocity-hodograph technique that are worth investigation. In particular, one can inspect the (effect of the) number of transfer revolutions N, the base functions, the degrees of freedom, departure date and TOF, etcetera.

First, we take a look at the influence of the number of revolutions for a particular situation: *i.e.* given departure date and velocity model. We derive the ΔV required as a function of TOF and number of revolutions N: Fig. 5.

Obviously, we obtain different curves for different values of N, and the outcome in terms of ΔV is not always consistent: for small TOF, $N = 0$ seems most attractive, whereas for larger values of this steering parameter $N = 3$ appears more feasible. It is clear that for a given model (*i.e.* given value of N), the required ΔV shows a smooth behavior, except for a small number of instances (separated, again, by the approximate synodic period for Earth-Mars). At such instances, a transfer-angle discontinuity occurs again. One can avoid the impact of this by switching to a problem formulation with a different value for N. So instead of keeping N fixed one increases N every time the transfer angle changes from 2π to 0, such that the final polar angle θ_f changes continuously. In this case it seems attractive to first (*i.e.* for small TOF) follow the solutions obtained with $N = 0$, then switch to solutions with $N = 1$ for higher TOF, then $N = 2$, and finally go after the ones obtained with $N = 3$.

Zero-order Solutions On a wider scale, one can do the exercise for a full grid of pairs of departure date and TOF, for a given set of velocity functions and number of revolutions. Fig. 6(a) shows the results for $N = 1$ (the color legend is explained in Fig. 7(a)). The results are clearly more-or-less repeating with synodic period, and attractive solutions (the blue parts of the plot) are found only for small TOFs. In a similar fashion, we can compute the ΔV required for $N = 2$: Fig. 6(b). Since plotted for the same grid and with the same color scale, we can readily observe that this option is more advantageous for many combinations of the steering parameters. Again, the repeating patterns are clearly distinguishable. Doing a similar exercise for $N = 0$, 3, 4, 5 and 6, one obtains similar plots with attractive and less-attractive sub-spaces. Being interested in minimum ΔV only, we subsequently overlay the seven plots and select the solution with the lowest propellant requirement for any pair in the grid (*i.e.* one of the seven possible solutions obtained for individual

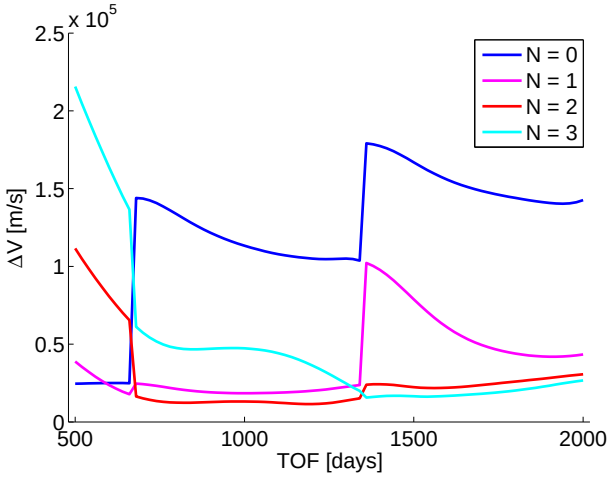

Figure 5. Optimal ΔV for different values for TOF for a mission to Mars, with different values for number of revolutions. Here, departure date is 7545 MJD2000 and V_r = CPowCosPCos, V_θ = CPowCosPSinPCos, V_z = CosR5Pow6P6CosR5.

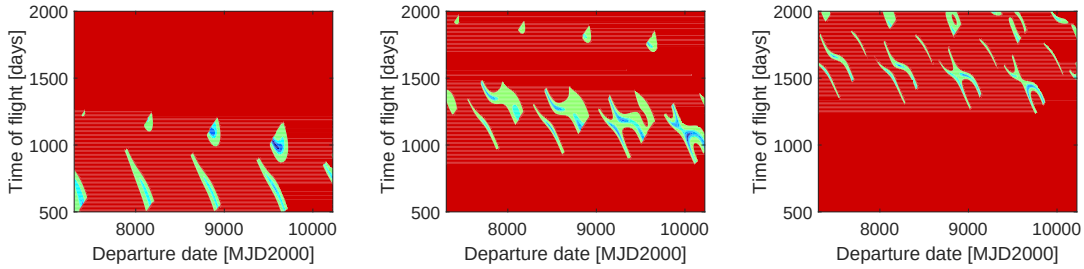

Figure 6. ΔV plot for the zero-order time-driven solution CPowPow2-CPowPow2-CosR5P3CosR5P3SinR5 for a mission to Mars with $N = 1$ (left), $N = 2$ (middle) and $N = 3$ (right).

N), and combine these best solutions in one plot: Fig. 7(a).

Clearly, Fig. 7(a) illustrates where the most interesting combinations of departure date and TOF are to be found. As discussed previously, such results to a large extent depend on the number of revolutions N. So, we can make another cross-section of the results in Fig. 7(a) by plotting them against two other parameters: ΔV and the maximum acceleration that is required to fly a particular trajectory. Since we can play around with the importance of each of these parameters, this is best expressed in a so-called Pareto front: Fig. 8. Fig. 5 suggested that there is no unique single-best solution for the number of revolutions, but when evaluated against the maximum acceleration f_{max} that is to be delivered by the rocket engine, we do have a consistent answer here: the best approach is to fly to Mars with $N = 2$. More precisely and at least for the velocity functions investigated here, this approach is most promising both in view of the maximum acceleration but also in terms of velocity change required.

So far, we have obtained the most attractive zero-order solution in terms of ΔV and maximum acceleration, which perfectly matches our rendezvous constraints on position, velocity and TOF. However, this result was derived for a specific set of velocity functions (see caption Fig. 8), and it

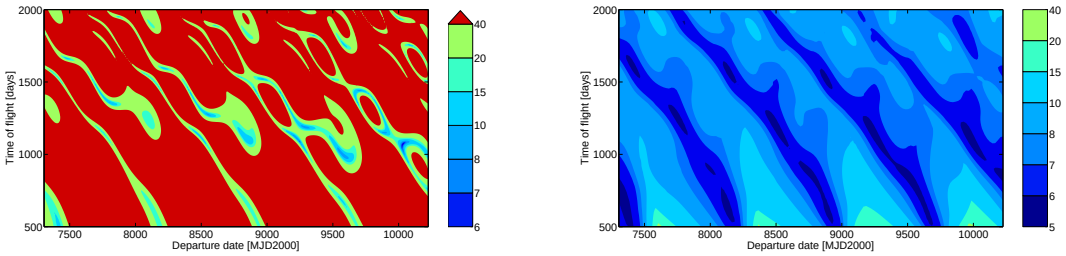

(a) Zero-order (b) Higher-order

Figure 7. ΔV plots for time-driven solutions CPowPow2-CPowPow2-CosR5P3CosR5P3SinR5 (left) and CPowPow2PSin05PCos05-CPowPow2PSin05PCos05-Cos25P3SinR5P3CosR5P4CosR5P4SinR5 (right) for a mission to Mars with $N = 0 - 6$.

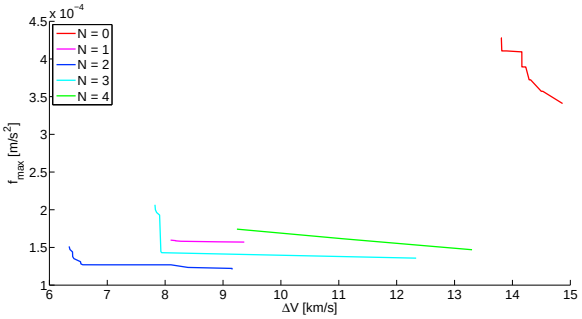

Figure 8. Pareto fronts of the zero-order time-driven solution CPowPow2-CPowPow2-CosR5P3CosR5P3SinR5 for different numbers of revolution for a mission to Mars.

can be expected that the choice of such functions will also play a role. To evaluate this, we have done a similar exercise for different velocity models, and summarized the results in Fig. 9 and Table 5.

One can immediately see that the modeling as shown by the green line in Fig. 9 performs best. Obviously, the modeling of the radial and transverse velocities on a mission to an outer planet like Mars is best off with power terms rather than trigonometric functions.

In a similar fashion, the consequences of the modeling of the axial velocity can be investigated. Simulating the axial velocity using an oscillating function with a changing amplitude was found to give the best results.[12]

Higher-order Solutions As mentioned earlier, the velocity-hodograph technique has the option to model the velocity functions with a larger number of base functions than strictly required by the number of constraints. The recipe for this is similar to what has been done for the zero-order solutions: play around with the base functions, the number of revolutions, departure date and TOF.

As an illustration, Fig. 7(b) shows the grid-search results for a particular combination of velocity functions. As was the case for the zero-order solutions, the effect of the (approximate) synodic period is visible again. More important, the regions with low ΔV correspond very well with the regions identified for the zero-order approach (Fig. 7(a)); however, the attractive regions for the higher-order solution are larger. So, the zero-order solutions can be used to give a reliable first

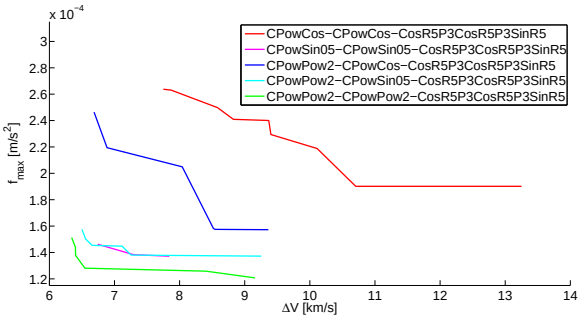

Figure 9. Pareto fronts of the zero-order time-driven solutions with different radial and transverse velocity functions for a mission to Mars. The axial velocity function is kept unchanged (see legend).

Table 5. Main characteristics of minimum-ΔV trajectories found by zero-order time-driven solutions with different radial and transverse velocity functions for a mission to Mars. The axial velocity function is kept to CosR5P3CosR5P3SinR5 for all cases considered here.

V_r	V_θ	Departure date [MJD2000]	TOF [days]	N [rev]	ΔV [km/s]	f_{max} [10^{-4} m/s^2]
CPowCos	CPowCos	9265	1070	2	7.751	2.64
CPowSin05	CPowSin05	10035	1070	2	6.742	1.46
CPowPow2	CPowCos	9245	1090	2	6.686	2.46
CPowPow2	CPowSin05	10025	1050	2	6.500	1.58
CPowPow2	CPowPow2	10025	1050	2	6.342	1.51

indication of the departure date and the TOF for more refined, optimal higher-order solutions, and hence reduce the search space that is to be covered by a more time-consuming optimization.

Shown from the more interesting perspective of ΔV and maximum required acceleration, the higher-order results are summarized again in a Pareto front: Fig. 10. To appreciate the results directly, the best zero-order solutions as well as results from independent sources[6,8] are also included.

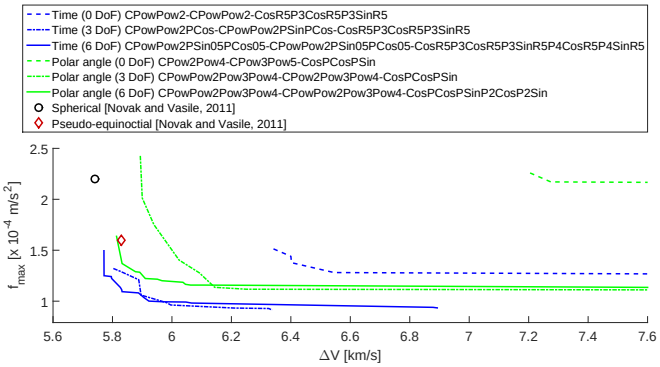

Figure 10. Pareto fronts of the best solutions for a mission to Mars.

As expected, the higher-order solutions clearly give better results regarding both ΔV and thrust acceleration. So, adding extra DoF results in better trajectories. This already holds when going from a zero-order velocity model to a 3-DoF formulation. The 6-DoF formulation gives best results,

though. Compared with the results obtained for spherical and pseudo-equinoctial shaping methods, the hodographic shaping method performs very well for a mission to Mars (see Fig. 10 and Table 6). The best ΔVs of the time-driven method are near-optimal (”near”, since it is a first-order method and we also worked with a limited resolution in our grid search) and the required thrust accelerations are feasible. Although not treated in detail here, the polar-angle driven results are of a bit poorer quality compared to those obtained with the time-driven implementation (Table 6). This is related to the “easy” characteristics of the Earth-Mars transfer.

Table 6. Required ΔV and maximum thrust acceleration for the minimum-ΔV trajectory found by different methods for a mission to Mars.

Method	ΔV [km/s]	f_{max} [10^{-4} m/s^2]
Hohmann	5.50	-
Hodographic - time	5.77	1.5
Hodographic - polar angle	5.81	1.6
Spherical[8]	5.74	2.2
Pseudo-equinoctial[8]	5.83	1.6
DITAN[7]	5.66	1.5

Finally, Fig. 11 shows the trajectory and thrust-acceleration profile of the best time-driven higher-order solution. The oscillating character of the axial-velocity function can be seen clearly in both the trajectory and the thrust-acceleration profile. A behavior like this is needed to achieve the inclination of Mars' orbit. In addition, the radial component of the thrust acceleration, which results in gravity losses, is very small; it indicates the near-optimality of the solution. Nevertheless the thrust-acceleration profile is non-optimal since it differs significantly from bang-bang control.

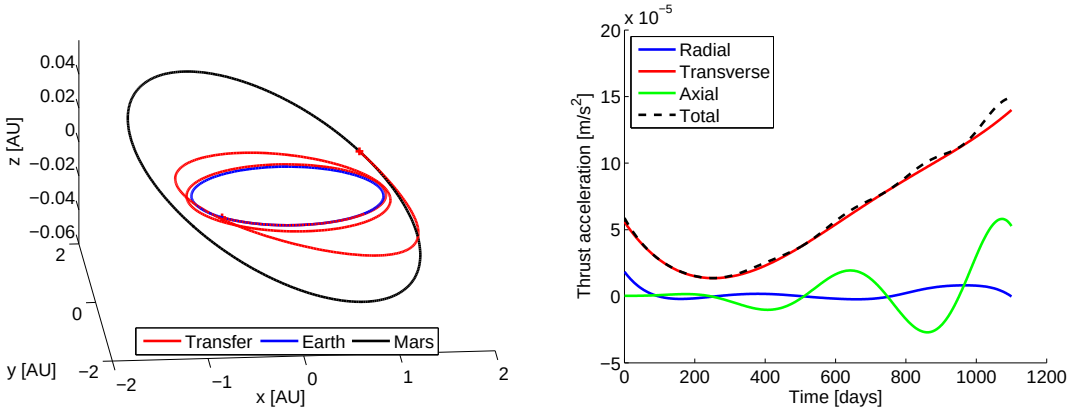

Figure 11. Trajectory (left) and thrust acceleration profile (right) of best higher-order time-driven solution for Earth-Mars: V_r = CPowPow2PSin05PCos05, V_θ = CPowPow2PSin05PCos05, V_z = CosR5P3CosR5P3SinR5P4CosR5P4SinR5, departure date is 9985 MJD2000 and TOF is 1100 days, see Table 6.

Mercury

The Mercury case is fundamentally different from the Mars case: it is an inner body with a significant eccentricity and inclination. For a mission to a more outer body the orbital period gradually

increases, and therefore even for long flight times only a few revolutions around the Sun suffice. However, on a transfer to a more inner target like Mercury, the "local" orbital period decreases, and a relatively large number of revolutions is needed to cover a long(er) transfer time. Also, a large TOF is required to achieve the target's eccentricity and inclination (certainly when being restricted in the maximum thrust that the rocket engine can supply). This makes Mercury an excellent test case to assess the many-revolution performance of the hodographic-shaping methods. As before, we will focus on the time-driven implementation, but results of the polar-angle-driven method will also be included - which turns out to be crucial.

Zero-order Solutions As with Mars, we begin with solutions for zero-freedom transfers, and investigate the optimal velocity functions and number of revolutions in particular. Figure 12 shows the Pareto front on ΔV and f_{max}, for various time-driven velocity modelings. As a general observation, a mission like this is on a different scale considering the much higher ΔV values, as well as the required (maximum) thrust acceleration which is an order of magnitude larger than in the Mars case. Similar to Mars though is the fact that the CPowPow2 model works best, since it provides the capability to have a quadratic behavior with time of the relevant velocity component. An inventory of the effect of the number of revolutions (not depicted here, the interested reader is referred to Gondelach[12]) revealed that for the best velocity model in Fig. 12 $N = 0$ is optimal. This is an undesired solution, because multiple revolutions would allow for a more gradual change of the orbit and therefore lower required thrust. These solutions are not feasible because of the high acceleration required and indicate that the time-driven method is not useful in this case. It turns out that the polar-angle-driven implementation performs better. For the axial velocity, it was found that a power order of eight (the maximum investigated) was best for all values of N. This is rather surprising, since it implies that the inclination change mainly takes place at the end of the trajectory where the spacecraft velocity is very high and such maneuvers are well known to be inefficient.

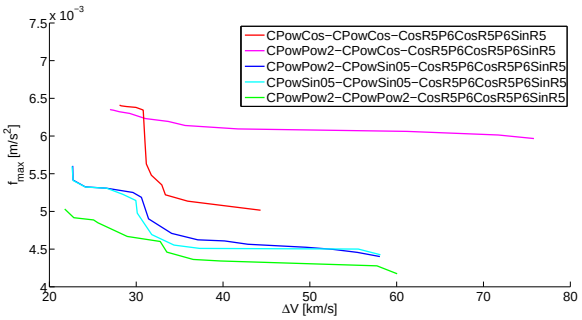

Figure 12. Pareto fronts of zero-order time-driven solutions for different radial- and transverse-velocity functions for a mission to Mercury.

Although not treated in detail here, we can do a similar exercise for the polar-angle-driven implementation of the hodograph technique. One of the results for the zero-order model is shown in Fig 13. The most noticeable observations are (again) the high value for ΔV, the repeating pattern (related to a synodic period of 116 days for Earth-Mercury), and the limited but clear regions that appear "attractive" from an energy point of view. The most interesting solutions have been obtained for $N = 2$, more in line with what is to be expected from a physical perspective.

Higher-order Solutions For this case as well, it is interesting to investigate whether improvements can be achieved when extra degrees of freedom are introduced. Fig. 14 shows such results, both for the time-driven and for the polar-angle-driven implementation. It is clear that the

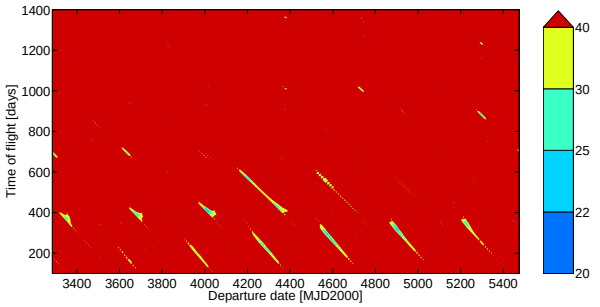

Figure 13. ΔV plot for polar-angle-driven zero-order solutions CPowPow3-CPow2Pow4-CosPCosPSin for a mission to Mercury with $N = 0 - 6$.

polar-angle-driven method performs better, especially regarding thrust acceleration, although the required rocket engine output is still high compared to the Mars case. Since the base functions in the polar-angle-driven method evolve with the polar angle, the velocity functions stay in sync with the strongly decreasing "local" orbital period when flying towards to Sun. The polar method is therefore more suitable to model trajectories for missions to inner targets than the time-driven method, especially when it comes to using multi-revolution trajectories.

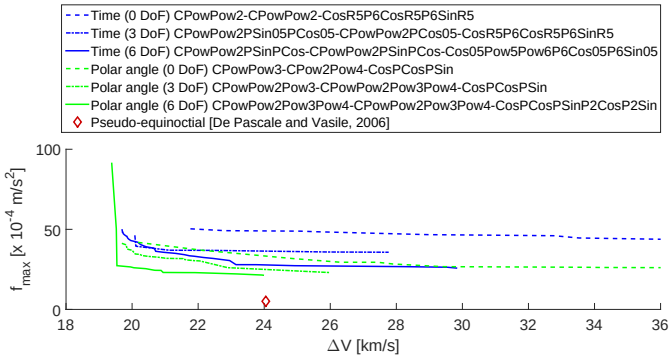

Figure 14. Pareto fronts of the best zero-order and higher-order solutions for a mission to Mercury.

To further illustrate the capabilities of the time-driven method, Fig. 15(b) shows the values for the required ΔV obtained with extra degrees of freedom, as usual for a range of departure dates and TOF. As before, the number of revolutions ranges between 0 and 6 (reflected in the TOF). For the given velocity model, the solutions presented here can be regarded as the best transfers that can be generated with the time-driven implementation of the velocity hodographs. It is obvious that the regions with acceptable solutions (*i.e.* with a "modest" ΔV) are quite restricted: narrow bands, clearly offset with respect to each other with the synodic period. The attractive subset of the solution space looks rather thin.

Contrary to this, Fig. 15(a) shows the ΔV that is required for the best higher-order polar-angle-driven implementation, as function of departure date and TOF. The trends as already observed with the zero-order polar-angle-driven (Fig. 13) and higher-order time-driven (Fig. 15(b)) solutions are clearly visible again. However, by virtue of the extra degrees of freedom and the improved suitability of the polar angle to describe attractive transfer trajectories, the mission can be flown for smaller amounts of ΔV and more attractive options are available, clearly: the subset of the search space

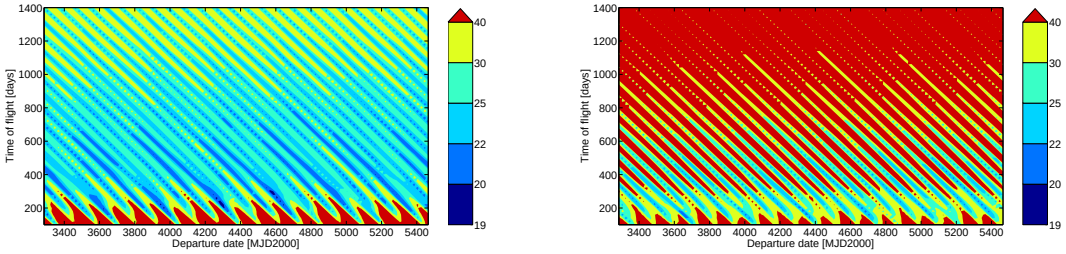

(a) Polar-angle-driven

(b) Time-driven

Figure 15. ΔV plots for the higher-order polar-angle-driven solution CPowPow2Pow3Pow4-CPowPow2Pow3Pow4-CosPCosPSinP2CosP2Sin (left) and time-driven solution CPowPow2PSin05PCos05-CPowPow2PSin05Cos05-CosR5P5CosR5P5SinR5P6CosR5P6SinR5 (right) for a mission to Mercury with $N = 0 - 6$.

with ΔV-values of less than 25 km/s is much larger, and it is even possible to identify regions with ΔV smaller than 20 km/s. Since many of these transfers have been generated with a number of full revolutions N up to 4, this makes the problem less sensitive to phasing of the target planet, and the current outcome (a more continuous subset of the search space) is as expected.

Again, this does not make the 0-DoF results useless; as before, they can be used to limit the search space for more time-consuming optimizations.

Finally, it is interesting to compare the best results obtained here with results found in literature: the pseudo-equinoctial method and DITAN.[6] This is done in Fig. 14 and Table 7. Compared with the external results, the hodographic-shaping methods perform well regarding ΔV, but poor in terms of f_{max}. However, the pseudo-equinoctial and DITAN results have been obtained including a constraint on the maximum thrust acceleration. So, trajectories which require less ΔV may be found by these methods if the thrust acceleration were not limited in size.

Table 7. Required ΔV and maximum thrust acceleration for the minimum-ΔV trajectory found by different methods for a mission to Mercury.

Method	ΔV [km/s]	f_{max} [10^{-4} m/s^2]
Hohmann	16.32	-
Hodographic - time	19.71	48.6
Hodographic - polar angle	19.38	91.2
Pseudo-equinoctial[6]	24.04	5.0
DITAN[6]	22.72	5.0

PREFERRED VELOCITY FUNCTIONS

Many different combinations of velocity functions have been tested for each case. The ones which gave good results in all cases (Mars and Mercury, but also comet Tempel 1 and asteroid 1989ML[12]) are shown in Table 8. These combinations are to be considered as reasonable-good starting points for any transfer problem, but of course tuning of the formulations could very well lead to (even) better results.

Table 8. Preferred velocity functions for 0 and 6 DoF.

Method	Radial	Transverse	Axial
t - 0 DoF	CPowPow2	CPowPow2	CosR5P3CosR5P3SinR5
t - 6 DoF	CPowPow2PSin05PCos05	CPowPow2PSin05PCos05	CosR5P3CosR5P3SinR5P4CosR5P4SinR5
θ - 0 DoF	CPow2Pow4	CPow3Pow5	CosPCosPSin
θ - 6 DoF	CPowPow2Pow3Pow4	CPowPow2Pow3Pow4	CosPCosPSinP2CosP2Sin

COMPUTATIONAL EFFORT

It has been shown that 0-DoF velocity models can provide reasonable solutions for transfer trajectories; however, their main characteristics can be improved by introducing extra degrees of freedom. Of course, this comes at a (computational) price, which is the topic of this section.

It was found that the required computation time depends on a number of aspects. Most important is the introduction of degrees of freedom: rather than providing a unique solution, it requires optimization and hence (much) more function evaluations. To a lesser extent the CPU time depends on the applied velocity functions and the number of revolutions. For example, (higher-order) power-times-trigonometric base functions require more time to evaluate than other base functions, since their integral is a series.[12] Also, for some combinations of TOF and number of revolutions it is very hard to find proper trajectories. This holds in particular for short flight times in combination with a large(r) number of revolutions.

Table 9. Average CPU times required to compute one trajectory for different methods and modelings (C++, Intel Core 2.27 GHz i5-430M processor, 64-bits Windows platform).

Method	Average computation time [ms]
Hodographic - t - 0 DoF	1.6
Hodographic - t - 3 DoF	8.2
Hodographic - t - 6 DoF	49
Hodographic - θ - 0 DoF	1.6
Hodographic - θ - 3 DoF	6.4
Hodographic - θ - 6 DoF	62
Spherical[8]	316
Pseudo-equinoctial[8]	238

Table 9 shows the average computation times for the different methods (averaged over the various test cases). Clearly the zero-order solutions are evaluated much faster (1.6 ms) than the high-order ones (up to 62 ms). For 0 DoF this means that the entire flight window for Mars for $N = 0 - 5$ (in total 67,000 points) can be analyzed within only 110 s. So, zero-order velocity models can identify regions in the flight window where the ΔV is low very quickly. Higher-order hodographic-shaping techniques require more computational effort, as expected, but this increment is only an order of magnitude higher. With respect to those of external techniques, the computational burden is quite favorable. However, it should be noted that a one-on-one comparison may not be valid, since the statistics for these have been taken from literature directly, and these computations have been done on different machines and with different coding techniques. Still, if only because of the smaller number of boundary conditions and the absence of iterations, 0-DoF hodographic shaping is most likely the fastest method irrespective of machine speed and coding language.

CONCLUSIONS

Based on shaping the velocity of a spacecraft during the transfer, a novel low-thrust trajectory design method has been developed. Here, velocity is represented by a sum of simple, analytical base functions. The latter can be differentiated and integrated analytically, such that the change in position can be expressed analytically and boundary conditions on position, velocity and time of flight can be met immediately, without iterations. A minimum of three base functions per coordinate direction (so nine in total) are required to satisfy all boundary conditions, and extra functions can be added to make the design and optimization of trajectories more flexible, with potentially better results.

Two different methods have been developed; one which shapes velocity as a function of time and another one (not treated in detail here) which shapes as a function of polar angle. The time-driven implementation appears very suitable for missions to more outer targets in the Solar System, whereas the polar-angle-driven version is favorable for missions to more inner objects. The computational times required for such calculations are very modest: they range from about 1.6 ms per trajectory evaluation for 0-DoF modelings to about 45 ms for modelings that include 6 extra degrees of freedom. Both the 0-DoF and the versions with extra degrees of freedom are particularly suited for a fast inventory of attractive flight opportunities for missions to arbitrary celestial targets.

REFERENCES

[1] A. E. Petropoulos and J. M. Longuski, "Automated Design of Low-Thrust Gravity-Assist Trajectories," *AIAA/AAS Astrodynamics Specialist Conference, AIAA Paper 2000-4033*, 2000, pp. 157–166.

[2] A. E. Petropoulos and J. M. Longuski, "Shape-based algorithm for automated design of low-thrust, gravity-assist trajectories," *Journal of Spacecraft and Rockets*, Vol. 41, No. 5, 2004, pp. 787–796.

[3] B. J. Wall, "Shape-based approximation method for low-thrust trajectory optimization," *AIAA/AAS Astrodynamics Specialist Conference and Exhibit, AIAA Paper 2008-6616, Honolulu, Hawaii*, 2008.

[4] B. J. Wall and B. A. Conway, "Shape-based approach to low-thrust rendezvous trajectory design," *Journal of Guidance, Control, and Dynamics*, Vol. 32, No. 1, 2009, pp. 95–102.

[5] B. J. Wall and D. M. Novak, "A 3D Shape-Based Approximation Method for Low-Thrust Trajectory Design," *Advances in the Astronautical Sciences Volume 142, AAS Paper 11-479*, 2012.

[6] P. De Pascale and M. Vasile, "Preliminary design of low-thrust multiple gravity-assist trajectories," *Journal of Spacecraft and Rockets*, Vol. 43, No. 5, 2006, pp. 1065–1076.

[7] M. Vasile, P. De Pascale, and S. Casotto, "On the optimality of a shape-based approach based on pseudo-equinoctial elements," *Acta Astronautica*, Vol. 61, No. 1-6, 2007, pp. 286–297.

[8] D. M. Novak and M. Vasile, "Improved shaping approach to the preliminary design of low-thrust trajectories," *Journal of Guidance, Control, and Dynamics*, Vol. 34, No. 1, 2011, pp. 128–147.

[9] O. Abdelkhalik and E. Taheri, "Shape Based Approximation of Constrained Low-Thrust Space Trajectories using Fourier Series," *Journal of Spacecraft and Rockets*, Vol. 49, No. 3, 2012, pp. 535–546.

[10] O. Abdelkhalik and E. Taheri, "Approximate On-Off Low-Thrust Space Trajectories Using Fourier Series," *Journal of Spacecraft and Rockets*, Vol. 49, No. 5, 2012, pp. 962–965.

[11] B. De Vogeleer, "Automatic and Fast Generation of Sub-optimal and Feasible Low-Thrust Trajectories Using a Boundary-Value Pseudo-Spectral Method," Master's thesis, TU Delft Repository, Delft University of Technology, Delft, Netherlands, August 2008.

[12] D. J. Gondelach, "A Hodographic-Shaping Method for Low-Thrust Trajectory Design," Master's thesis, TU Delft Repository, Delft University of Technology, Delft, Netherlands, July 2012.

[13] D. J. Gondelach and R. Noomen, "Hodographic-Shaping Method for Low-Thrust Interplanetary Trajectory Design," *Journal of Spacecraft and Rockets*, Vol. 52, No. 3, 2015, pp. 728–738.

[14] R. O'Neill, "Algorithm AS 47: Function Minimization Using a Simplex Procedure," *Journal of the Royal Statistical Society. Series C (Applied Statistics)*, Vol. 20, No. 3, 1971, pp. 338–345.